10.1515/msr-2015-0007

MEASUREMENT SCIENCE REVIEW, Volume 15, No. 1, 2015

Analytical Modeling for the Grating Eddy Current Displacement Sensors

Chunfeng Lv[1], Wei Tao[2], Huaming Lei[2], Yingying Jiang[2], Hui Zhao[2]

[1]College of Engineering Science and Technology, Shanghai Ocean University, Shanghai, 201306, China, chunfenglvluyi@gmail.com,

[2]Department of Instrument Science and Engineering, Shanghai Jiao Tong University, Shanghai, 200240, China, taowei@sjtu.edu.cn, hmlei@sjtu.edu.cn, yayadanlian@sjtu.edu.cn, huizhao@sjtu.edu.cn (corresponding author)

As a new type of displacement sensor, grating eddy current displacement sensor (GECDS) combines traditional eddy current sensors and grating structure in one. The GECDS performs a wide range displacement measurement without precision reduction. This paper proposes an analytical modeling approach for the GECDS. The solution model is established in the Cartesian coordinate system, and the solving domain is limited to finite extents by using the truncated region eigenfunction expansion method. Based on the second order vector potential, expressions for the electromagnetic field as well as coil impedance related to the displacement can be expressed in closed-form. Theoretical results are then confirmed by experiments, which prove the suitability and effectiveness of the analytical modeling approach.

Keywords: Grating eddy current sensor, analytical modeling, displacement measurement.

1. INTRODUCTION

EDDY CURRENT TESTING is a nondestructive technique working on the principle of electromagnetic induction, based on which the eddy current sensors are widely used in many industrial fields such as metal defect detection, vibration testing and displacement measurement, etc. Compared to other types of displacement sensors, eddy current displacement sensors have their own outstanding characteristics of water and dust proof, simple structure, high sensitivity and so on. Although the eddy current displacement sensors have those prominent features, measuring range is an unavoidable restraining factor for further expanding the application area. Displacement measured by traditional eddy current sensors is usually the liftoff of the coil relative to the reflective conductor, and the measuring range is mainly determined by the coil dimensions such as radius of circular coils or length and width of rectangular coils [1-3]. In practical applications, however, it is impossible to enlarge the measuring range by merely increasing the coil sizes. For this reason, it is very meaningful and necessary to develop new types of eddy current displacement sensors which can perform a wide range measurement without changing properties of the coil.

From grating type displacement sensors such as grating optical sensors, grating magnetic sensors and grating capacitance sensors [4-6], the whole measuring range is composed of many measuring units, which are also named as measuring cycles. Therefore, the final displacement value is the summation of the absolute value in one measuring cycle and numbers of the cycles. In this way, wide measuring range estimation without any precision reduction can thus be carried out. This paper proposes a type of grating eddy current displacement sensor (GECDS) which combines the eddy current sensor with grating structure. In contrast to traditional eddy current displacement sensors, the GECDS consists of a series of reflective conductors which form a grating configuration type by arranging them equidistantly. While the coil moves along the orientation of these conductors, impedance of the testing coil will change periodically. Moreover, the testing coil integrates the functions of exciting with pickup, which simplifies the coil design and sensor structure.

In order to obtain the output characteristics such as coil impedance variation of the GECDS, various approaches including analytical modeling methods or pure numeric methods are adopted for computational analysis of the eddy current problem. Among these methods, analytical modeling approaches can provide solutions in closed-form expressions since they are directly performed through solving the Maxwell equations. Therefore, analytical approaches have definite physical meanings, and this is extremely useful for researchers learning the essence of the eddy current phenomena. In addition, computing time of analytical approaches is much less than that of pure numeric methods. In the paper, basic measurement principles of the GECDS are firstly introduced, and then a complete structure of the GECDS is provided. Through establishing a theoretical model of the GECDS in the Cartesian coordinate system, closed-form expression for variation of coil impedance is obtained from the truncated region eigenfunction expansion (TREE) method. Finally, absolute positioning method of the GECDS is provided.

2. THE GECDS

As shown in Fig.1., the GECDS consists of a testing coil and a number of reflective conductors. The coil is placed parallel to the conductors with a fixed distance d and it can move transversely relative to the conductors. Width of each conductor along the moving direction is $\lambda/2$, and these

conductors are arranged with a fixed distance λ from a grating structure. Thus, the whole measuring range is divided into many measuring cycles with the width of λ, and each measuring cycle is named as a measuring period.

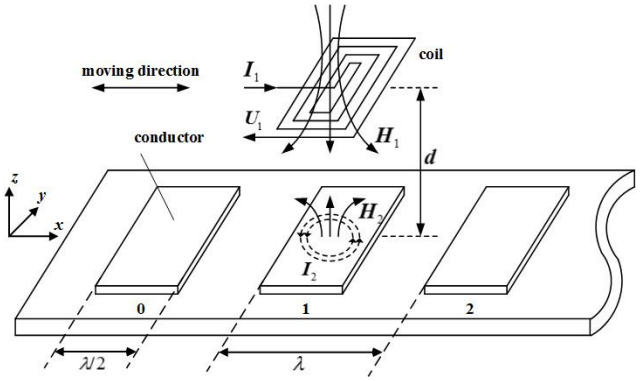

Fig.1. Basic structure of the GECDS.

While the coil moves transversely, coupling area between the coil and conductors will change, which makes impedance of the coil change accordingly. Taking one measuring period into account, when the testing coil is directly over the conductor (conductor 1 in Fig.1.), eddy current induced in conductors acting on the coil makes the inductance of the coil minimum. Inductance value reaches maximum while the coil is at the middle position between conductors 1 and 2 due to the weakest eddy current effects, and then it reaches minimum again when the coil is over the conductor 2. In a whole measuring period, variation of the coil inductance is thus a repetitive process of minimum to maximum and to minimum again. Therefore, wide range measurement is performed through measuring the absolute position of the coil in one measuring period and adding numbers of the periods.

In practical use, however, it is difficult to accurately obtain absolute position only using one coil. In order to solve this problem, a differential structure with multicoils is adopted, which is shown in Fig.2. Width of each coil along the moving direction is the same as that of one conductor, which is $\lambda/2$. Coil 1 and coil 2 are $\lambda/2$ apart form a set of differential coils. In a similar way, coil 3 and coil 4 form another pair of differential coils, and these two sets of differential coils are $\lambda/4$ apart from each other. Moreover, coils 1, 2, 3 and 4 are all composed of six subcoils with the same sizes, respectively. These subcoils are connected in series from end to end with a fixed interval which equals to one measuring period λ. With the layout strategy of these subcoils, self-inductance of the coil can be increased with fewer layers while it is fabricated by the printed circuit board (PCB) techniques, which is cost-effective of fabrication. The differential structure can not only increase the resolution but also improve the capacity of resisting disturbance [7].

During the measurement, the two output signals of coil 1 and 2 form a differential signal by subtraction, and another differential signal is formed by coils 3 and 4 using the same method. Absolute displacement value can thus be calculated from these two differential signals. Absolute positioning method will be introduced in the following sections after the coil inductance variation against displacement from the analytical modeling approach is derived.

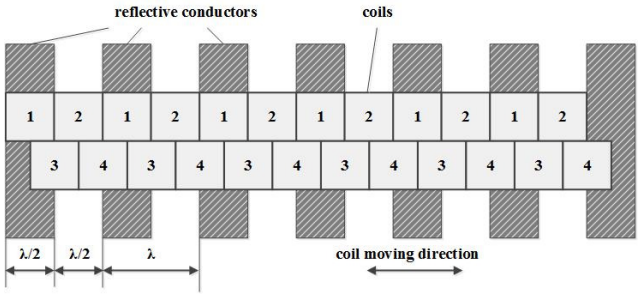

Fig.2. Layout of the GECDS.

3. ANALYTICAL MODELING FOR THE GECDS IN THE CARTESIAN COORDINATE SYSTEM

In order to obtain the change law of the coil impedance related to the displacement, take coil 1 as an illustration. An original solving model for one measuring period of the GECDS is shown in Fig.3. The six subcoils connected in series in Fig.2. are equivalent to one single coil, and it can be treated as a rectangular coil with rectangular cross section.

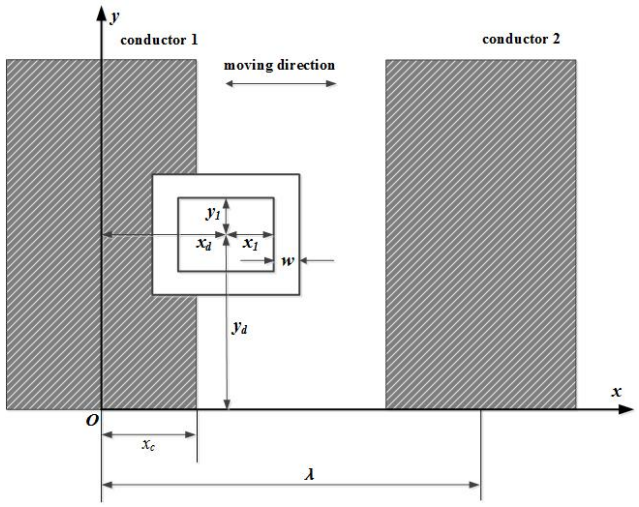

Fig.3. Solving model of the GECDS within one measuring period.

While the coil is moving within a measuring period, suppose firstly that the coil is only affected by two conductors, and the mutual inductance between these two conductors can be disregarded due to the spacing distance between them. Secondly, variation of the coil impedance is worked out when the conductor 1 alone is acting on the coil. For the conductor 2, since it is actually an inverse symmetry process relative to conductor 1, variation of the coil impedance can then be determined using the same method. Finally, a complete coil impedance variation process under

the coaction of these two conductors within a measuring period is thus obtained through the superposition method. Moreover, each conductor in the model is a conductive plate with right-angle wedge, and it is regarded as a conductive quarter space which is different from the conductive half space in traditional models [3, 8].

A. Scalar decomposition using second order vector potential

The electromagnetic (EM) field interrelated to the GECDS can be expressed in terms of the second order vector potential (SOVP) in the Cartesian coordinate system [9]. Using the scalar decomposition, the magnetic flux density is

$$\mathbf{B} = \nabla \times \nabla \times \mathbf{W} \tag{1}$$

$$\mathbf{W} = \mathbf{e}_x W_a + \mathbf{e}_x \times W_b \quad , \tag{2}$$

where $\mathbf{e}_x$ denotes the unit vector of x direction, W_a and W_b are the transverse electric (TE) and transverse magnetic (TM) scalar potentials, respectively. These two scalar potentials satisfy the Laplace or Helmholtz equations corresponding to the nonconductive and conductive regions

$$\nabla^2 \begin{bmatrix} W_a \\ W_b \end{bmatrix} = k^2 \begin{bmatrix} W_a \\ W_b \end{bmatrix} \tag{3}$$

For the conductive region there is $k^2 = j\omega\mu_0\mu_r\sigma$, in which $\omega = 2\pi f$ is the angular frequency corresponding to the excitation frequency f of the coil. μ_0, μ_r and σ are the vacuum permeability, relative permeability and electrical conductivity of the conductor, respectively.

Components of the magnetic flux density in the Cartesian coordinate system from (2) are

$$B_x = \frac{\partial^2 W_a}{\partial x^2} - k^2 W_a \tag{4}$$

$$B_y = \frac{\partial^2 W_a}{\partial x \partial y} + k^2 \frac{\partial W_b}{\partial z} \tag{5}$$

$$B_z = \frac{\partial^2 W_a}{\partial x \partial z} - k^2 \frac{\partial W_b}{\partial y} \tag{6}$$

Especially for the nonconductive region where $k^2 = 0$, the magnetic flux density can be expressed as the gradient of the TE potential

$$\mathbf{B} = \nabla\left(\frac{\partial W_a}{\partial x}\right) \tag{7}$$

B. The TREE method and Symmetric solutions

As mentioned earlier, the whole process of the coil impedance variation within a measuring period is a combined result of which conductor 1 and 2 is acting alone on the coil, respectively. The initial problem can be simplified to such a solving model only with one conductor (conductor 1 in Fig.3.), from which variation of the coil impedance is calculated. As for conductor 2, coil impedance variation is the inverse symmetric process from that of the conductor 1.

For the solving model with one conductor, the TREE method means the solving domain is limited to finite extents by imposing artificial boundaries in both x and y directions. These boundaries can be set as a magnetic insulator (normal component of the magnetic flux density is zero) or an electric insulator (tangential component of the magnetic field is zero). Furthermore, from the symmetric consideration, only half of the original truncated domain is needed to be considered through adding an auxiliary boundary at $x = 0$. The initial problem is then decomposed to even or odd solution [10]. For even solution, the boundary at $x = 0$ is a magnetic insulator, which indicates current flow in the coil and its image coil mirrored at $x \le 0$ is in the same direction. While for odd solution, current flow in the two coils is in the opposite directions, which makes the boundary at $x = 0$ an electric insulator. The final solution is the average summation of the two solutions. Fig.4. shows the simplified solving model within finite extents, and the boundary conditions are as follows: boundaries at $x = a_x$ and $y = b_y$ are the magnetic insulator, and boundary at $y = 0$ is the electric insulator.

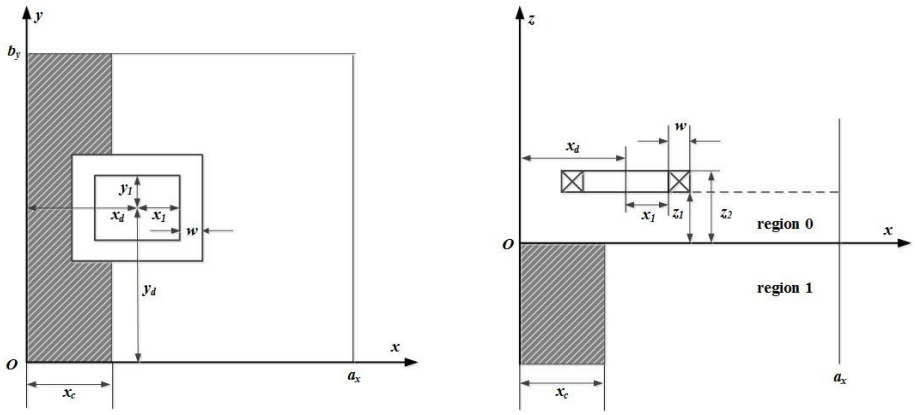

Fig.4. Solving model in a truncated domain.

C. Even solution

In the nonconductive region 0, the magnetic flux density is only related to the gradient of the TE potential from (7), and it satisfies the Laplace equation. This potential is expressed as a superposition of the source coil and reaction of the eddy current induced within the conductor

$$\frac{\partial W_a^{(0)}}{\partial x} = \frac{\partial W_a^{(s)}}{\partial x} + \frac{\partial W_a^{(ec)}}{\partial x} \tag{8}$$

From the boundary conditions for even solution, these two potentials are written

$$\frac{\partial W_a^{(s)}}{\partial x} = \sum_{n=1}^{\infty}\sum_{m=1}^{\infty} \sin(v_n y)\cos(u_m x) C_{mn}^{(s)} \exp(\gamma_{mn} z) \tag{9}$$

$$\frac{\partial W_a^{(ec)}}{\partial x} = \sum_{n=1}^{\infty}\sum_{m=1}^{\infty} \sin(v_n y)\cos(u_m x) D_{mn}^{(ec)} \exp(-\gamma_{mn} z), \tag{10}$$

where $u_m = m\pi / a_x$, $v_n = (2n-1)\pi / (2b_y)$ and $\gamma_{mn}^2 = u_m^2 + v_n^2$

The source coefficient $C_{mn}^{(s)}$ is related to the coil properties such as shape, size and excitation current, and the coefficient $D_{mn}^{(ec)}$ is the expansion coefficient needed to be solved in the nonconductive region 0.

The source coefficient $C_{mn}^{(s)}$ is determined by the excitation current I and geometric parameters shown in Fig.4. According to the superposition method [3, 11], the source coefficient of the rectangular coil with rectangular cross section is

$$C_{mn}^{(s)} = \frac{8\mu_0 NI}{a_x b_y w(z_2 - z_1)} \sin(v_n y_d)\cos(u_m x_d) \times \frac{\exp(-\gamma_{mn} z_1) - \exp(-\gamma_{mn} z_2)}{\gamma_{mn}} \frac{\Gamma_R}{u_m v_n}, \tag{11}$$

where N denotes number of the coil turns, x_d is the displacement value, $y_d = b_y / 2$ ensures the coil far from the two boundaries in y direction, and $\Gamma_R = \int_0^w \sin[u_m(x_1 + w)]\sin[v_n(y_1 + w)]dw$.

For the region 1($z \le 0$) which includes the conductive and air region, the TE and TM potentials are written

$$W_a^{(1)} = \begin{cases} \sum_{n=1}^{\infty}\sum_{m=1}^{\infty} \sin(v_n y)\sin(q_m x) \times C_{mn}^{(a)con} \exp(\lambda_{mn} z) & 0 \le x \le x_c \\ \sum_{n=1}^{\infty}\sum_{m=1}^{\infty} \sin(v_n y)\sin[p_m(a_x - x)] \times C_{mn}^{(a)air} \exp(\lambda_{mn} z) & x_c \le x \le a_x \end{cases} \tag{12}$$

where $\lambda_{mn}^2 = q_m^2 + v_n^2 + k^2 = p_m^2 + v_n^2$, and the expansion coefficients $C_{mn}^{(a)con}$ and $C_{mn}^{(a)air}$ are the conductive and air subregions in region 1, respectively.

For the TM potential W_b in region 1, it is only related within the conductive region. Notice that the normal component of the current density is zero at the conductor-air interface $x = x_c$, the TM potential is expressed

$$W_b^{(1)} = \sum_{n=1}^{\infty}\sum_{m=1}^{\infty} \cos(v_n y)\cos(r_m x) C_{mn}^{(b)} \exp(s_{mn} z), \tag{13}$$

where $r_m = (2m-1)\pi / (2x_c)$, $s_{mn}^2 = r_m^2 + v_n^2 + k^2$, and $C_{mn}^{(b)}$ is the expansion coefficient which is needed to be solved.

From (12), the continuity conditions at the interface $x = x_c$ are written

$$\sin(q_m x_c) C_{mn}^{(a)con} = \sin[p_m(a_x - x_c)] C_{mn}^{(a)air} \tag{14}$$

$$q_m \cos(q_m x_c) C_{mn}^{(a)con} = -p_m \cos[p_m(a_x - x_c)] C_{mn}^{(a)air} \tag{15}$$

An auxiliary coefficient a_m is used subsequently to express the relationship between the two expansion coefficients $C_{mn}^{(a)con}$ and $C_{mn}^{(a)air}$ in (12), which is $a_m C_{mn}^{(a)con} = C_{mn}^{(a)air}$, and it is written from (14) and (15)

$$a_m = \frac{\sin(q_m x_c)}{\sin[p_m(a_x - x_c)]} = -\frac{q_m \cos(q_m x_c)}{p_m \cos[p_m(a_x - x_c)]} \tag{16}$$

The two eigenvalues p_m and q_m can thus be calculated from (16) with $q_m = \sqrt{p_m^2 - k^2}$

$$p_m \tan(q_m x_c) + q_m \tan[p_m(a_x - x_c)] = 0 \tag{17}$$

In the following steps, a numerical scheme is adopted to calculate these two eigenvalues. Two limiting cases are needed to be considered with respect to the width of the conductor x_c . One is the incrementing case, and another is the decrementing case. For the incrementing case, suppose firstly that $x_c = 0$, and the eigenvalue $p_m = u_m$ which indicates that the conductor vanished and this is the same condition for finding u_m . Then, width of the conductor is increased step by step in a small increment Δx_c until it reaches the true value x_c . In each step, the Newton-Raphson iteration algorithm is used to compute the eigenvalues, which is

$$p_m^{i+1} = p_m^i - \frac{f(p_m)^i}{\left|\frac{df(p_m)}{dp_m}\right|^i}, \tag{18}$$

where $f(p_m) = p_m \tan(q_m x_c) + q_m \tan[p_m(a_x - x_c)]$, and i is the iteration number. For a particular value of x_c, the eigenvalue can be obtained while p_m^{i+1} differs from p_m^i by a very small amount. Next, the eigenvalue for a new value of $x_c + \Delta x_c$ can be computed from the previous step for x_c. Therefore, after the value reaches the true width of x_c, it provides one set of eigenvalues.

For the decrementing case, the iteration is started at $x_c = a_x$, and the starting eigenvalue changes to $p_m = \sqrt{u_m^2 + k^2}$. In this case, x_c is decreased step by step until it reaches the true value x_c again, and in each decrementing step the Newton-Raphson iteration algorithm is also used. Like the incrementing case, one can obtain another set of eigenvalues. Consequently, the final set of eigenvalues is therefore obtained by merging these two sets of eigenvalues computed from the incrementing and decrementing case. The eigenvalues used for computations are the ones from a specific index number m.

After obtaining the expression of TE and TM potentials in each region, the next step is to work out the unknown expansion coefficients from the continuity conditions of the magnetic field. Substituting (8) into (4) to (6), the three components of the magnetic flux density in region 0 are

$$B_x^{(0)} = \sum_{n=1}^{\infty}\sum_{m=1}^{\infty} \sin(v_n y)\sin(u_m x) \times (-u_m)[C_{mn}^{(s)} \exp(\gamma_{mn} z) + D_{mn}^{(ec)} \exp(-\gamma_{mn} z)] \quad (19)$$

$$B_y^{(0)} = \sum_{n=1}^{\infty}\sum_{m=1}^{\infty} \cos(v_n y)\cos(u_m x) \times v_n[C_{mn}^{(s)} \exp(\gamma_{mn} z) + D_{mn}^{(ec)} \exp(-\gamma_{mn} z)] \quad (20)$$

$$B_z^{(0)} = \sum_{n=1}^{\infty}\sum_{m=1}^{\infty} \sin(v_n y)\cos(u_m x) \times (\gamma_{mn})[C_{mn}^{(s)} \exp(\gamma_{mn} z) + D_{mn}^{(ec)} \exp(-\gamma_{mn} z)] \quad (21)$$

Components of the magnetic flux density in region 1 are

$$B_x^{(1)} = \begin{cases} \sum_{n=1}^{\infty}\sum_{m=1}^{\infty} \sin(v_n y)\sin(q_m x) \times (-p_m^2) C_{mn}^{(a)con} \exp(\lambda_{mn} z) & 0 \le x \le x_c \\ \sum_{n=1}^{\infty}\sum_{m=1}^{\infty} \sin(v_n y)\sin[p_m(a_x - x)] \times (-p_m^2) a_m C_{mn}^{(a)con} \exp(\lambda_{mn} z) & x_c \le x \le a_x \end{cases} \quad (22)$$

$$B_y^{(1)} = \begin{cases} \sum_{n=1}^{\infty}\sum_{m=1}^{\infty} \cos(v_n y)[\cos(q_m x) q_m v_n C_{mn}^{(a)con} \exp(\lambda_{mn} z) + k^2 \cos(r_m x) s_{mn} e^{s_{mn} z} C_{mn}^{(b)} \exp(s_{mn} z)] & 0 \le x \le x_c \\ \sum_{n=1}^{\infty}\sum_{m=1}^{\infty} \cos(v_n y)\cos[p_m(a_x - x)] \times (-p_m v_n) a_m C_{mn}^{(a)con} \exp(\lambda_{mn} z) & x_c \le x \le a_x \end{cases} \quad (23)$$

$$B_z^{(1)} = \begin{cases} \sum_{n=1}^{\infty}\sum_{m=1}^{\infty} \sin(v_n y)[\cos(q_m x) q_m \lambda_{mn} C_{mn}^{(a)con} \exp(\lambda_{mn} z) + k^2 \cos(r_m x) v_n C_{mn}^{(b)} \exp(s_{mn} z)] & 0 \le x \le x_c \\ \sum_{n=1}^{\infty}\sum_{m=1}^{\infty} \sin(v_n y)\cos[p_m(a_x - x)] \times (-p_m \lambda_{mn}) a_m C_{mn}^{(a)con} \exp(\lambda_{mn} z) & x_c \le x \le a_x \end{cases} \quad (24)$$

From the expressions of the EM field listed above, they all satisfy the continuity conditions at the plane $z = 0$. It can be written in the matrix form through the use of orthogonality for trigonometric functions

$$\frac{a_x}{2}\mathbf{u}(\mathbf{C}_n^{(s)} + \mathbf{D}_n^{(ec)}) = \mathbf{M}_s \mathbf{C}_n^{(a)con} \quad (25)$$

$$\frac{a_x}{2} v_n (\mathbf{C}_n^{(s)} + \mathbf{D}_n^{(ec)}) = v_n \mathbf{M}_c \mathbf{C}_n^{(a)con} + k^2 \mathbf{M}_r \mathbf{s}_n \mathbf{C}_n^{(b)} \quad (26)$$

$$\frac{a_x}{2} \boldsymbol{\gamma}_n (\mathbf{C}_n^{(s)} - \mathbf{D}_n^{(ec)}) = \mathbf{M}_c \boldsymbol{\lambda}_n \mathbf{C}_n^{(a)con} + k^2 v_n \mathbf{M}_r \mathbf{C}_n^{(b)} \quad (27)$$

For each v_n, $\mathbf{C}_n^{(s)}$, $\mathbf{D}_n^{(ec)}$, $\mathbf{C}_n^{(a)con}$ and $\mathbf{C}_n^{(b)}$ are the column vectors, and $\mathbf{u}$, $\boldsymbol{\gamma}_n$, $\boldsymbol{\lambda}_n$ and $\mathbf{s}_n$ are the diagonal matrices corresponding to u_m, q_m and s_m. The other three matrices $\mathbf{M}_s$, $\mathbf{M}_c$ and $\mathbf{M}_r$ are square matrices

$$\mathbf{M_s}[i,j] = p_j^2 \int_0^{x_c} \sin(u_i x)\sin(q_j x)dx + p_j^2 a_m \int_{x_c}^{a_x} \sin(u_i x)\sin[(p_j(a_x - x)]dx \quad (28)$$

$$\mathbf{M_c}[i,j] = q_j \int_0^{x_c} \cos(u_i x)\cos(q_j x)dx - p_j a_m \int_{x_c}^{a_x} \cos(u_i x)\cos[(p_j(a_x - x)]dx \quad (29)$$

$$\mathbf{M_r}[i,j] = q_j \int_0^{x_c} \cos(u_i x)\cos(r_j x)dx \ , \quad (30)$$

where $i = 1,2,3\cdots m$, $j = 1,2,3\cdots m$, and they are determined by the summation terms of the series.

Therefore, all the expansion coefficients can be derived through solving the three equations (25) to (27) with the known source coefficient $C_{mn}^{(s)}$. For instance, the coefficient $D_{mn}^{(ec)}$ which is used for calculating the coil impedance is

$$\mathbf{D}_n^{(ec)} = -\mathbf{C}_n^{(s)} + \frac{2}{a_x}\mathbf{u}^{-1}\mathbf{M}_s\mathbf{C}_n^{(a)con} \tag{31}$$

D. Odd solution

For odd solution, the only difference is the additional boundary condition at $x = 0$, which changes into the electric insulator. With other boundary conditions unchanged, and notice that the derivation steps are the same as those of the even solution, expressions of the TE and TM potentials are as follows:
In region 0:

$$\frac{\partial W_a^{(0)}}{\partial x} = \frac{\partial W_a^{(s)}}{\partial x} + \frac{\partial W_a^{(ec)}}{\partial x}$$
$$= \sum_{n=1}^{\infty}\sum_{m=1}^{\infty}\sin(v_n y)\sin(u_m x)[C_{mn}^{(s)}\exp(\gamma_{mn} z) + D_{mn}^{(ec)}\exp(-\gamma_{mn} z)] \tag{32}$$

where $u_m = (2m-1)\pi/(2a_x)$, $v_n = (2n-1)\pi/(2b_y)$ and $\gamma_{mn}^2 = u_m^2 + v_n^2$. $D_{mn}^{(ec)}$ is the expansion coefficient needed to be solved, and the source coefficient is

$$C_{mn}^{(s)} = \frac{8\mu_0 NI}{a_x b_y w(z_2 - z_1)}\sin(v_n y_d)\sin(u_m x_d) \times \frac{\exp(-\gamma_{mn} z_1) - \exp(-\gamma_{mn} z_2)}{\gamma_{mn}}\frac{\Gamma_R}{u_m v_n} \tag{33}$$

In region 1, the TE and TM potentials are written

$$W_a^{(1)} = \begin{cases} \sum_{n=1}^{\infty}\sum_{m=1}^{\infty}\sin(v_n y)\cos(q_m x) \times C_{mn}^{(a)con}\exp(\lambda_{mn} z) & 0 \le x \le x_c \\ \sum_{n=1}^{\infty}\sum_{m=1}^{\infty}\sin(v_n y)\sin[p_m(a_x - x)] \times a_m C_{mn}^{(a)con}\exp(\lambda_{mn} z) & x_c \le x \le a_x \end{cases} \tag{34}$$

$$W_b^{(1)} = \sum_{n=1}^{\infty}\sum_{m=1}^{\infty}\cos(v_n y)\sin(r_m x)C_{mn}^{(b)}\exp(s_{mn} z) \ , \tag{35}$$

where $\lambda_{mn}^2 = q_m^2 + v_n^2 + k^2 = p_m^2 + v_n^2$, $r_m = m\pi/x_c$, $s_{mn}^2 = r_m^2 + v_n^2 + k^2$, $C_{mn}^{(a)con}$ and $C_{mn}^{(b)}$ are the expansion coefficients.
The auxiliary coefficient a_m in this case is

$$a_m = \frac{\cos(q_m x_c)}{\sin[p_m(a_x - x_c)]} = \frac{q_m \sin(q_m x_c)}{p_m \cos[p_m(a_x - x_c)]} \tag{36}$$

The eigenvalues can be obtained using the same method described in the even solution from

$$q_m \tan(q_m x_c) - p_m \cot[p_m(a_x - x_c)] = 0 \tag{37}$$

Derivations of the unknown coefficients in odd solution are in the same form as (25) to (27). Therefore, through changing the eigenfunctions and eigenvalues corresponding to the boundary conditions for the odd solution and substituting them into those equations listed above, expansion coefficients for odd solution are worked out following the same steps provided in the even solution.

4. COMPUTATIONAL RESULTS AND ABSOLUTE POSITIONING METHOD

A. Variation of the coil inductance

Since the eddy current effects induced within the conductors reacting on the coil are different at various coil positions within a measuring period, impedance of the coil will keep changing while the coil moves transversely. From Fig.2., coil 1 which consists of six subcoils connected in series is deemed to be a single coil in Fig.3. and Fig.4. Therefore, the final calculation result for this equivalent coil equals to the summation results of the six subcoils.

Expression for the variations of the coil impedance is calculated from [12]

$$\Delta Z = \frac{1}{\mu_0 I^2}\iint_S \mathbf{e}_z \cdot (\mathbf{E}^{(s)} \times \mathbf{H}^{(0)} - \mathbf{E}^{(0)} \times \mathbf{H}^{(s)})dS \ , \tag{38}$$

where S denotes a closed surface at z = 0 closed within the truncated domain in x and y directions, and it extends to the region at z<0. $\mathbf{E}^{(0)}$ and $\mathbf{H}^{(0)}$ are the electric and magnetic field not including the conductor, while $\mathbf{E}^{(s)}$ and $\mathbf{H}$(s) are the field including the conductor. The expression (38) can be written in terms of the TE potential in the nonconductive region

$$\Delta Z = -\frac{j\omega}{\mu_0 I^2}\int_0^{b_y}\int_0^{a_x}\left(\frac{\partial W_a^{(ec)}}{\partial x}\frac{\partial W_a^{(s)}}{\partial x\partial z} - \frac{\partial W_a^{(s)}}{\partial x}\frac{\partial W_a^{(ec)}}{\partial x\partial z}\right)\Big|_{z=0} dxdy \tag{39}$$

From the Parseval's theorem and expressions of the $W_a^{(s)}$ and $W_a^{(ec)}$ for even and odd solutions, the final expression for the impedance change is

$$\Delta Z = -\frac{j\omega a_x b_y}{2\mu_0 I^2}\sum_{n=1}^{\infty}\sum_{m=1}^{\infty}\gamma_{mn} C_{mn}^{(s)} D_{mn}^{(ec)} \tag{40}$$

This is a general expression and it is suited for both the even and odd solutions. The coil impedance is only related

to the transverse displacement value x_d while keeping other parameters unchanged.

For the TREE method, as mentioned earlier, artificial boundaries a_x and b_y should be imposed far from the coil and conductor. In this paper, the truncated domain is set as $a_x = b_y = nx_c$ with $n = 20$ and the summation terms of the series is $2n$, which ensures accuracy of the calculation results. Sizes of the subcoil in Fig.3. and testing parameters are listed in Table 1.

Table 1. Sizes of the subcoil and testing parameters.

Coil sizes		Testing parameters	
x_1	0.5mm	f	3.2MHz
y_1	0.5mm	σ	14.6MS/m
w	0.75mm	μ_r	1
z_1	0.5mm	x_c	1.25mm
z_2	1.3mm	λ	5mm
N	20		

Fig.5. shows the change tendency of the coil inductance within one measuring period, from which one can find the change law of the coil inductance related to the displacement.

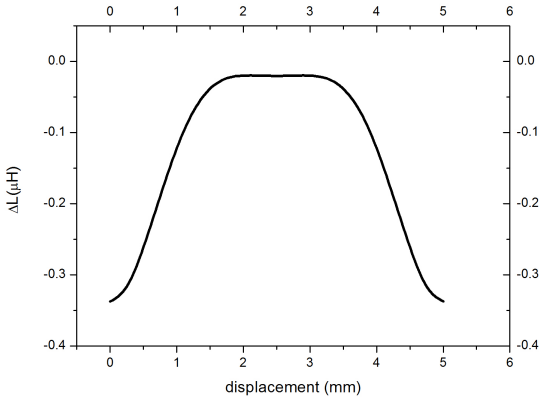

Fig.5. Variation curve of the coil inductance within a measuring period.

For the purpose of fast and accurate measuring of the coil impedance against the displacement, an indirect approach using the LC oscillator circuit is adopted. Output frequency signal will change due to the coil inductance variation. The frequency signal is measured by the synchronous counters built in the micro control unit. Relationship between the frequency f and the coil inductance L is

$$f = 1/(2\pi\sqrt{LC}) \quad , \tag{41}$$

where $L = L_0 + \Delta L$ is the instantaneous inductance of the coil, which includes the self-inductance L_0 and inductance variation ΔL of the coil. Total self-inductance of the six subcoils measured by a digital bridge device is $L_0 = 3.81\mu\text{H}$. The equivalent capacitance of the oscillator is $C = 650\,\text{pF}$.

For the verification of the calculated results, the calculated results are converted to the frequency signal from (41). Theoretical and experimental results of the frequency variation curves within two measuring periods are shown in Fig.6. It can be seen from the figure that the two curves are fitted well, and they both have the same variation period and rules.

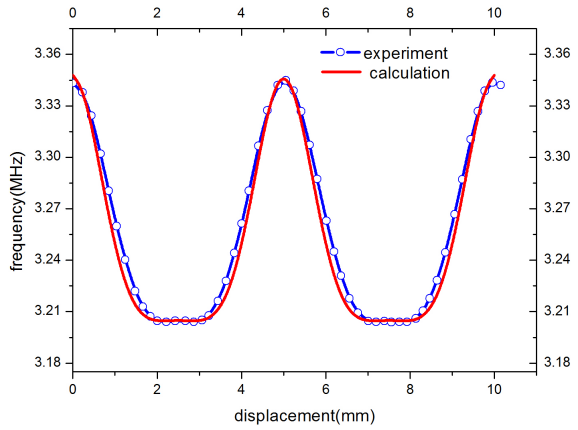

Fig.6. The experimental and calculated results of the frequency.

B. Absolute displacement in one measuring period

As mentioned in the previous section, two differential signals should be used for absolute positioning in one measuring period. Inductance variation of coils 2, 3 and 4 can be derived from the computing results of coil 1 through shifting it by $\lambda/2$, $\lambda/4$ and $3\lambda/4$, respectively. The two differential signals L_{12} and L_{34} are expressed as

$$L_{12} = \Delta L_2 - \Delta L_1 \tag{42}$$

$$L_{34} = \Delta L_4 - \Delta L_3 \tag{43}$$

Results of coil inductance in the two measuring periods are shown in Fig.7.

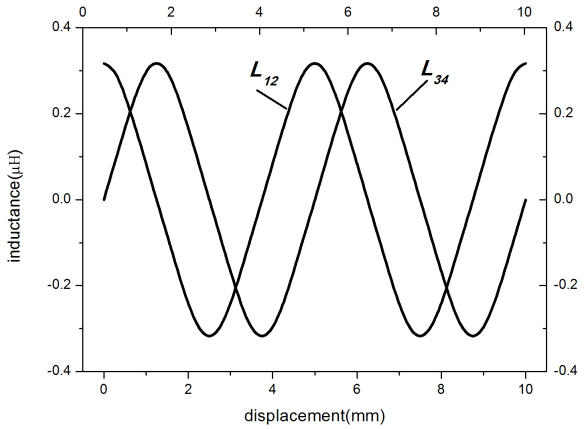

Fig.7. Variation of the two differential inductance curves.

It can be seen from the figure that these two differential curves approach the cosine and sinusoidal curve, respectively, which can be roughly expressed

$$L_{12} = A\cos(2\pi x_d / \lambda) \tag{44}$$

$$L_{34} = A\sin(2\pi x_d / \lambda) \quad , \tag{45}$$

where A is the amplitude of the signal, and x_d is the displacement value in Fig.3. Then the phase angle is calculated from

$$\varphi = \arctan(L_{34} / L_{12}) \tag{46}$$

Linear variation of the phase angle related to the displacement within two measuring periods is shown in Fig.8. according to (46).

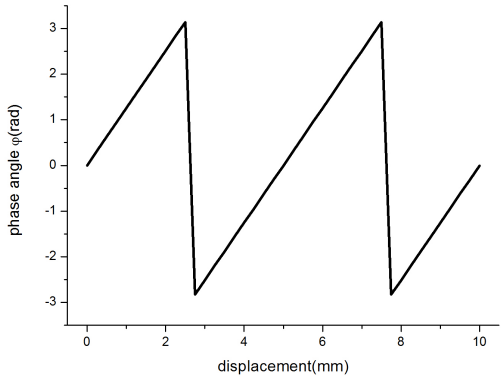

Fig.8. Linear variation curve between phase angle and displacement.

The absolute displacement value x_d can thus be obtained from (46)

$$x_d = \lambda\varphi / 2\pi \tag{47}$$

Assuming that the number of the measuring periods K has been acquired, the total displacement D equals to $K\lambda + x_d$.

5. CONCLUSION

The GECDS combining the grating structure and accuracy of traditional eddy current sensors performs the function of wide range measurement without precision reduction, which has broad perspectives in application. The analytical modeling approach proposed in this manuscript analyzes the coil impedance variation of the GECDS. Therefore, one can investigate effects of the sensor parameters, such as axial gap between coils and reflective conductors, excitation frequency and the coil dimensions from the angle of this theoretical mode. Both these parameters determine the performance of the GECDS including sensitivity, nonlinearity error and so on. Therefore, an effective multi-parameter optimization method based on this model is imperative for economic and efficient production, and this is one of the research goals of the future works.

ACKNOWLEDGMENT

This work is supported by National Natural Science Foundation of China (61362017, 61365007). The authors sincerely thank Professor Theodoros Theodoulidis for his generous assistance during the work, and they also appreciate the anonymous reviewers for their valuable comments on the work.

REFERENCES

[1] Moulder, J.C., Uzal, E., Rose, J.H. (1992). Thickness and conductivity of metallic layers from eddy current measurements. *Review of Scientific Instruments*, 63 (6), 3455-3465.

[2] Fava, J.O., Ruch, M.C. (2006). Calculation and simulation of impedance diagrams of planar rectangular spiral coils for eddy current testing. *NDT and E International*, 39 (5), 414-424.

[3] Theodoulidis, T.P., Kriezis, E.E. (2002). Impedance evaluation of rectangular coils for eddy current testing of planar media. *NDT and E International*, 35 (6), 407-414.

[4] Frazão, O., Ferreira, L.A., Araújo, F.M., Santos, J.L. (2005). Applications of fiber optic grating technology to multi-parameter measurement. *Fiber and Integrated Optics*, 24 (3-4), 227-244.

[5] Ambrosino, C., Campopiano, S., Cutolo, A., Cusano, A. (2008). Sensitivity tuning in Terfenol-D based fiber Bragg grating magnetic sensors. *IEEE Sensors Journal*, 8 (9), 1519-1520.

[6] Hall, N.A., Lee, W., Dervan, J., Degertekin, F.L. (2002). Micromachined capacitive transducers with improved optical detection for ultrasound applications in air. In *IEEE Ultrasonics Symposium*. IEEE, Vol. 2, 1027-1030.

[7] Weiwen, L., Hui, Z., Hongli, Q. (2009). Research on novel grating eddy-current absolute-position sensor. *IEEE Transactions on Instrumentation and Measurement*, 58 (10), 3678-3683.

[8] Theodoulidis, T., Bowler, J.R. (2010). Interaction of an eddy-current coil with a right-angled conductive wedge. *IEEE Transactions on Magnetics*, 46 (4), 1034-1042.

[9] Smythe, W.R. (1968). *Static and Dynamic Electricity*. New York: McGraw-Hill, 284-296.

[10] Theodoulidis, T.P., Kriezis, E.E.(2006). *Eddy Current Canonical Problems (with Applications to Nondestructive Evaluation)*.Tech Science Press.

[11] Dodd, C.V., Deeds, W.E. (1968). Analytical solutions to eddy-current-probe-coil problems. *Journal of Applied Physics*, 39 (6), 2829-2838.

[12] Auld, B.A., Muennemann, F., Winslow, D.K. (1981). Eddy current probe response to open and closed surface flaws. *Journal of Nondestructive Evaluation*, 2 (1), 1-21.

Received June 15, 2014.
Accepted January 30, 2015.